Van der Waals density-functional study of 100% hydrogen coverage on bilayer graphene

R.E. Mapasha,[1,*] R.C. Andrew,[1,†] and N. Chetty[1,2]

[1]*Physics Department, University of Pretoria, Pretoria 0002, South Africa*
[2]*National Institute for Theoretical Physics, Johannesburg, 2000, South Africa*

(Dated: May 9, 2013)

We investigate all hydrogen configurations that exist in a 1×1 unit cell of bilayer graphene at 100% coverage to find the low energy competing configurations using density functional theory (DFT). Other unique configurations, obtained from a 2×1 supercell, are also investigated. The GGA-PBE functional and four variants of non-local van der Waals density functionals namely, vdW-DF, vdW-DF2, vdW-DF-C09$_x$, and vdW-DF2-C09$_x$ are used to account for the exchange correlation effects. Ten unique hydrogen configurations are identified for 1×1 unit cell bilayer graphene, and nine of these structures are found to be energetically stable with three low energy competing configurations. One arrangement found to exist in both 1×1 and 2×1 cell sizes is the most energetically stable configuration of all considered. For some of the configurations identified from the 2×1 supercell, it is found that the effect of hydrogenation results in greatly distorted hexagonal layers resulting in unequal bond distances between the carbon atoms. Also, interaction between the hydrogen-decorated planes greatly affects the energetics of the structures. The vdW-DF-C09$_x$ functional is found to predict the shortest interlayer distances for all the configurations, whereas the GGA-PBE functional predicts the largest. For the most energetically favorable configuration, hydrogenation is found to reduce the elastic properties compared with pristine bilayer graphene.

PACS numbers: 68.43.Bc, 68.43.Fg, 73.22.Pr

I. INTRODUCTION

Density functional theory (DFT) is one of the most reliable and widely used electronic structure methods. Its ability to correctly describe a wide range of condensed materials has attracted the attention of a large number of scientists and engineers. The well known local density approximation and generalized gradient approximation functionals (LDA and GGA-PBE) accurately describe covalent and ionic bonded networks, but fail to completely capture the effects of van der Waals (vdW) forces in complex systems. For the graphite structure, LDA gives a relatively good interlayer distance between layers but a poor binding energy,whereas GGA-PBE gives physically meaningless values.

To resolve these issues, scientists have made significant efforts in developing new exchange correlation functionals that are compatible with the Kohn Sham equations while incorporating the long-range effects of van der Waals forces.[1–7] One such functional was developed by Dion *et al.*[1] in 2004 and is known as the van der Waals density functional (vdW-DF). The vdW-DF functional consists of three exchange correlation energy terms, viz. (1) a non-local correlation energy E_c^{nl} given by

$$E_c^{nl} = \frac{1}{2}\int\int n(\mathbf{r})n(\mathbf{r}')\phi(\mathbf{r},\mathbf{r}')d^3r d^3r', \qquad (1)$$

where $\phi(\mathbf{r},\mathbf{r}')$ is the vdW-DF kernel which depends on the distance $|\mathbf{r}-\mathbf{r}'|$, the charge density and its gradient, (2) the local-density approximation correlation term E_c^{LDA} and (3) the revised Perdew Burke and Enzerhof[8] (revPBE) exchange energy term E_x^{revPBE}. Using the algorithm developed by Soler *et al.*,[9] vdW-DF shows its efficiency in describing a wide range of systems without demanding too much computational cost. Calculations for graphite indicate that vdW-DF correctly predicts the weak binding energy between layers but overestimates the interlayer distance when compared to experimental results. This overestimation is due to the repulsive nature of the revPBE exchange term. In 2010, Klimes *et al.*[10] and Cooper[11] constructed a new exchange functional (C09$_x$) to replace the strongly repulsive revPBE exchange term. The resulting vdW-DF-C09$_x$ functional shows an improvement in the calculated interlayer distance but an overestimation in the binding energy of graphitic systems, i.e. graphite and bilayer graphene.[12] In 2010, Lee *et al.*[13] improved the non-local correlation term of vdW-DF to obtain better binding energies. This improved functional is called vdW-DF2 and contains a refitted Perdew-Wang PW86R exchange functional term.[14] They later combined vdW-DF2 with C09$_x$ to develop vdW-DF2-C09$_x$ which addressed the overestimated interlayer distances and binding energies obtained with vdW-DF and vdW-DF-C09$_x$, respectively.[12,13]

In this study, we investigate the performance of the vdW-DF2-C09$_x$ functional to describe the energetics and structural properties of hydrogenated bilayer graphene and compare its performance to that of the GGA-PBE, vdW-DF, vdW-DF2, and vdW-DF-C09$_x$ functionals. Bilayer graphene consists of two stacked graphene layers bonded together by vdW forces. Graphene, a free standing layer of graphite, has drawn the attention of many researchers following its synthesis by Novoselov *et al.* in 2004.[15] Graphene and bilayer graphene are fascinating materials because of their unique electronic properties. The energy bands of single layer graphene at low energies are described by a two dimensional Dirac equation with a linear energy-momentum dispersion near the K point of the Brillouin zone.[16–22] The electrons are comparable to quasiparticles with an effective speed of 10^6 m/s, giving graphene excellent properties such as an anomalous quantum Hall effect (QHE) at room temperature and the ballistic transport of massless Dirac Fermions.[17,19] In bilayer graphene, the π linear dispersion splits into two parabolic bands near the K point.[23,24]

This split is a result of the strong interlayer coupling between the stacked layers, and demonstrates the possibility of easily tuning the band structure.[23–25] These novel structures form the backbone of future carbon based electronic devices.

The semi-metallic nature of these two materials limits their direct technological applications in as much as the fabrication of carbon based electronic devices is concerned. This issue of zero band gap has attracted much attention leading to efforts to engineer the band gap. Several methods have been employed to alter the electronic properties of these materials[26–34,37,40] with adsorption[35–50] being the most commonly used technique and hydrogen as the favored adatom. A wide band gap of about 3.5 eV has been observed experimentally[49] and calculated theoretically.[38,41,50] Numerous studies have already been conducted on hydrogen atoms adsorbed on single layer graphene but there is little information about hydrogen on bilayer graphene. A possible reason for this could be the failure of the standard GGA-PBE functional to correctly describes the vdW forces binding the layers of the bilayer graphene structures.

Subrahmanyam *et al.*[51] conducted some experimental studies of the adsorption of hydrogen on monolayer and few-layer graphene. Their spectroscopic studies revealed the existence of sp^3 re-hybridization bonding in the hydrogenated few-layer graphene. Jaiswal *et al.*[52] used a combination of charge transport and Raman spectroscopy experiments to study the adsorption of hydrogen on bilayer graphene. Different degrees of hydrogenation where considered to examine the electronic properties of hydrogenated monolayer and bilayer graphene. They deduced that partially hydrogenated structures have weak insulating behavior and also that bilayer graphene is quite susceptible to adsorption of hydrogen atoms compared to single layer graphene. Lately, Wang *et al.*[53] performed experimental studies of the physisorption of H_2 molecules on graphene at low and high surface coverages. Their calculated heats of adsorption indicated that high surface coverage was favored leading them to conclude that graphene has a high hydrogen storage capability. Several theoretical studies on the hydrogenation of bilayer graphene have been considered at low coverages.[41,54,55] Recently, Rohrer *et al.*[56] performed van der Waals density functional (vdW-DF) studies on the adsorption of hydrogen atoms on bilayer graphene and bulk graphite at 100% coverage. Their results demonstrated that vdW interactions can alter the electronic behavior in the Brillouin zone. They also found that the engineered band gap is caused by two geometry-induced effects, viz. (1) the hybridization between unoccupied wavefunctions in the lowest conduction band, and (2) the modification of the electrostatic interaction between hybrid wavefunctions and the total density.

It is known that hydrogenation of single layer graphene at 100% coverage only allows for two hydrogen configurations, i.e. (1) all the hydrogen atoms are adsorbed above the layer, (2) half of the hydrogen atoms are above and the remaining half is adsorbed below arranged in an alternating pattern. This is true for a 1×1 unit cell that contains only two atoms, but when the cell is made larger there are many other possible configurations. In this study, we use the GGA-PBE, vdW-DF, vdW-DF2, and vdW-DF-C09$_x$,vdW-DF2-C09$_x$ functionals to examine the structural properties for all the hydrogen configurations that can possibly exist in a 1×1 unit cell of bilayer graphene with 100% coverage and find the lowest energy competing configurations. Thereafter, we increase the size of the cell to 2×1 to show other energetically stable configurations at 100% that are not possible in the 1×1 cell. Lastly, the effect of hydrogen on the elastic properties of one of the most energetically favorable configurations is examined.

This paper is organized as follows: In section II we present the computational methodology and the parameters used. In section III, we discuss our results, and we summarize these results and draw conclusions in section IV.

II. METHODOLOGY

Our calculations were carried out using a plane-wave basis set and the projector augmented wave (PAW)[57] pseudopotential method as implemented in the PWscf code included in the Quantum ESPRESSO package.[58] The calculations were performed using the GGA-PBE,[59] vdW-DF, vdW-DF2, vdW-DF-C09$_x$ and vdW-DF2-C09$_x$ functionals. For the expansion of the wavefunctions, an energy cut-off of 500 eV was set for the plane wave basis. We used the Monkhorst-Pack scheme[60] with a grid of size 10×10×1 to sample the Brillouin zone. For SCF self-consistency, an energy convergence threshold was set at 10^{-7} eV. The atoms were allowed to relax, using the conjugate gradient algorithm, until the forces were less than 0.002 eV/Å. We employed a 1×1 and 2×1 cell for the construction of the bilayer graphene structures, with a vacuum spacing of 30 Å to reduce the interactions between periodic, vertical bilayer graphene images. The equilibrium lattice constants and interlayer distances for pristine bilayer graphene were obtained using all the above mentioned functionals, and were found to be in agreement with previous results.[55,61]

III. RESULTS AND DISCUSSION

A. Identification of possible hydrogen adatoms configurations on bilayer graphene

Fig. 1 shows (a) a 1×1 unit cell and (b) a 2×1 supercell for *AB* (Bernal) stacked bilayer graphene that we have used to identify possible hydrogen configurations. The labels (a, b, a′ and b′) show the possible distinct carbon atoms on the bilayer graphene. The symbols a_a and a_b show the hydrogen adsorbed at position x above and below the carbon atoms labelled a, etc. Since we consider 100% coverage, all the carbon atoms in each identified configuration are hydrogenated. By relaxing the ten unique configurations identified from the 1×1 unit cell (listed in Table I), we see that the relaxed configurations, apart from configurations C_7-C_9, appear to be completely different from their initial unrelaxed state because of the formation of H_2 dimers.

Hydrogen dimers occur for configurations where two hydrogen atoms are placed, on the same side, on top of the two distinct carbon atoms at positions x (in the unrelaxed

state). Such configurations are severely energetically unstable in their unrelaxed state but are stabilized by the H_2 dimer effect after relaxation. During relaxation, these hydrogen atoms simultaneously detach from the layer and attract each other resulting in the formation of a H_2 dimer. Configurations C_3-C_6 yield interesting geometries because of the mixture of chemisorption and physisorption. We therefore perform a thorough investigation of these structures.

We further constructed the 2×1 supercell that contains four atoms per plane (layer) to examine the properties of other configurations that are not possible in a 1×1 unit cell. The configurations identified are referred to as C_{11}-C_{16}, also presented in Table I. Some of these configurations where first studied by Leenearts *et. al.*[62] considering single layer graphene. In C_{11}-C_{13}, the chair, zigzag and boat conformers are observed as shown on Fig. 3, respectively. It must be mentioned that configurations C_{14}-C_{16} contain combinations of pairs of the various conformers as presented in Table I. The energetics of these configurations are examined and discussed in the next section.

B. Stability analysis and structural properties

To examine the relative stabilities of the identified configurations, the formation energy of each configuration is calculated. The formation energy (E_f), is defined as the energy per atom of the hydrogenated bilayer graphene with respect to intrinsic graphene and the corresponding H_2 dimer, i.e. $E_f = [E_{H-b} - N_C \times E_G - N_H \times E_{H_2}]/N_C$, where E_{H-b}, E_G and E_{H_2} are the energies per atom of relaxed, hydrogenated bilayer graphene, intrinsic graphene, and a H_2 dimer, respectively. N_C and N_H denote the total number of carbon and hydrogen atoms in the 1×1 unit cell respectively. Fig. 4 shows the formation energies per carbon for all identified hydrogen configurations on bilayer graphene using all five exchange correlation functionals. It is observed that for all identified configurations, the GGA-PBE functional predicts the highest formation energies as compared to those functionals with the non-local vdW density functional corrections.

Out of the ten uniquely identified configurations from 1×1 unit cell, Fig. 4 shows that, nine of these structures, C_1-C_9 are energetically favorable while C_{10} is not. The relaxed local structure of C_{10} shows that only one carbon atom on each plane is hydrogenated (see Fig. 2(e)). This configuration has the highest formation energy of 0.968 eV/atom (GGA-PBE), 0.865 eV/atom (vdW-DF), 0.699 eV/atom (vdW-DF2), 0.508 eV/atom (vdW-DF-C09$_x$) and 0.705 eV/atom (vdW-DF2-C09$_x$). It is therefore energetically expensive to experimentally synthesis C_{10}. The effects of the vertically oriented H_2 dimer physisorbed between the two planes does not reduce the formation energy of this structure. It is suggested that under conditions of finite temperature, structures similar to C_{10} may become energetically favorable.[38]

Fig. 4 shows that amongst all energetically favorable configurations, the employed exchange correlation functionals predict C_1 and C_2 to be less stable than C_3-C_9. It is observed that the adsorption occurring in configurations C_1 and C_2 is the physisorption of H_2 dimers as seen in Fig. 2 (a and b) whereas that in C_3-C_9 is either chemisorption or both. The observed low formation energies in C_3-C_9 arise from the planes where chemisorption has occurred. For configurations C_1 and C_2, GGA-PBE gives the small, positive formation energies of 0.062 eV/atom and 0.059 eV/atom respectively whereas the non-local vdW density functional corrections give negative formation energies of -0.150 eV/atom (vdW-DF), -0.331 eV/atom (vdW-DF2), -0.314 eV/atom (vdW-DF-C09$_x$) and -0.106 eV/atom (vdW-DF2-C09$_x$) for C_1 and -0.156 eV/atom (vdW-DF), -0.331 eV/atom (vdW-DF2), -0.364 eV/atom (vdW-DF-C09$_x$) and -0.120 eV/atom (vdW-DF2-C09$_x$) for C_2. These values indicate viable metastability of these two structures. Based on these formation energies, C_2 is more energetically favorable than C_1. The presence of the H_2 dimer between the two graphene layers in C_1, decouples the structure leading to a large interlayer separation of 7.92 Å (GGA-PBE), 6.55 Å (vdW-DF), 6.38 Å(vdW-DF2), 6.27 Å(vdW-DF-C09$_x$) and 6.31 Å(vdW-DF2-C09$_x$). The significant variation between the GGA-PBE functional and the vdW variants is attributed to the vdW force interaction arising between the observed H_2 dimer and the decoupled layers. In C_2, the interlayer separation of 4.11 Å (GGA-PBE), 3.51 Å (vdW-DF), 3.49 Å (vdW-DF2), 3.28 Å (vdW-DF-C09$_x$) and 3.29 Å (vdW-DF2-C09$_x$) still retains the pristine (graphitic) value (see Fig. 5). The relative equilibrium interlayer distances Δd (calculated with respect to pristine bilayer graphene) of C_2 is effectively zero. We conclude that the H_2 dimers physisorbed outside the bilayer have no effect on the vdW forces holding the layers together.

In Fig. 4, it is observed that configurations C_3-C_6 have less formation energies than C_1 and C_2 but higher than C_7-C_9. These configurations, i.e. C_3-C_6 are grouped together because they have both chemisorption and physisorption. The strong covalent bond between the carbon and hydrogen atoms that causes a complete depuckering in plane A, and the weak vdW interactions between H_2 dimer and the flat plane B seen in Fig. 2(c and d) are responsible for the intermediate stabilities of these configurations. It is important to note that configurations C_3 is equivalent to C_4 with the hydrogen adsorption sites on plane A swapped (see Table I). The three functionals vdW-DF, vdW-DF-C09$_x$ and vdW-DF2-C09$_x$ show that C_3 is 0.002eV/atom lower in formation energy than C_4. Configuration C_5 is 0.001 eV/atom (GGA-PBE), 0.003 eV/atom (vdW-DF), 0.003 eV/atom (vdW-DF2), 0.004 eV/atom (vdW-DF-C09$_x$), 0.003 eV/atom (vdW-DF2-C09$_x$) lower in formation energy than C_6. We therefore give a detailed discussion of the difference in properties between C_3 and C_5.

From our calculated formation energy values, we observe that the energy of C_3 is higher than that of C_5 by 0.001 eV/atom (GGA-PBE), 0.006 eV/atom (vdW-DF), 0.015eV/atom (vdW-DF2), 0.006eV/atom vdW-DF-C09$_x$, 0.005 eV/atom (vdW-DF2-C09$_x$). This difference in formation energy is not significant whereas the major difference is observed in the interlayer separations. Configuration C_3 is a decoupled structure with large interlayer separations of 12.67 Å (GGA-PBE), 7.86 Å (vdW-DF), 8.64 Å (vdW-DF2), 6.44 Å (vdW-DF-C09$_x$) and 6.75 Å (vdW-DF2-C09$_x$), caused

by the effect of atomic hydrogen bonded to plane A and a physisorbed H_2 dimer between the layers. Configuration C_5 has an interlayer separation of 4.68 Å (GGA-PBE), 4.16 Å (vdW-DF), 3.98 Å (vdW-DF2), 3.97 Å (vdW-DF-C09$_x$) and 3.91 Å (vdW-DF2-C09$_x$). The relative interlayer distance Δd in configuration C_5 shows that the effect of atomic hydrogen adsorbed on plane A, within the interlayer region, increases the interlayer separation by only 0.58 Å (GGA-PBE), 0.65 Å (vdW-DF), 0.47 Å (vdW-DF2), 0.69 Å (vdW-DF-C09$_x$) and 0.62 Å (vdW-DF2-C09$_x$). We suggest that C_5 is still coupled, and therefore more stable than the decoupled configuration C_3. This is also indicated by the coupled configuration C_2 being more stable than the decoupled C_1. It suffices to mention that the effect of vdW interactions within bilayer graphene greatly affect the energetics of these systems.

In Table II, we present the variations in the distances between the H_2 dimers and the planes. The GGA-PBE functional predicts that the H_2 dimer binds at a distance of about 3.90 Å away from the layer (measured either inside (I) or outside (O) the bilayer). This value suggests that the dimer is further away from the layer compared to that predicted by non-local vdW corrections where the dimer is about 2.80 Å (which is in agreement with LDA results[63]). It must be noted that the LDA results were obtained when a H_2 dimer was physisorbed on single layer graphene. Since it is well known that the H_2 dimer interacts with graphitic structures through a typical π-involved weak interaction, we expect the vdW functionals to predict better distances, particularly the recently developed vdW-DFs with the exchange functional (C09$_x$) of Cooper, namely, (vdW-DF-C09$_x$) and (vdW-DF2-C09$_x$). It has been observed that, in general, vdW-DF-C09$_x$ and vdW-DF2-C09$_x$ predict small distances.[12] These small values are attributed to the use of the exchange functional C09$_x$, since the vdW-DF correlation with in place of the repulsive revPBE exchange term overestimates interlayer separations.[12] It is also observed in Table II that all the functionals predict the separation d_{C-H_2} measured inside the layers (I) to be less than the d_{C-H_2} measured outside (O). This is not surprising since at position (I), both layers are attempting to reach their equilibrium separation and are hindered by the presence of the dimer whereas at (O), the dimer is free to adjust its position away from the outer layer.

Fig. 4 shows that configurations C_7-C_9 are the lowest energy competing geometries as compared to others. Atomic arrangements of these configurations show that all the hydrogen atoms are covalently bonded with the carbon atoms after relaxations. We also compare the formation energies of these configurations with that of graphane (a fully hydrogenated graphene monolayer where hydrogen atoms are arranged in an alternating pattern). It is noted in Fig. 4 that their formation energies are nearly the same. We further construct a 2×1 supercell of bilayer graphene to show that there are several physically interesting configurations that are not possible for a 1×1 unit cell. Six unique energetically favorable configurations are identified and presented in Table I. It is noted that configuration C_{11} has a similar hydrogen arrangement (chair-like) as C_7-C_9 (see Fig. 3). All of these configurations have the same buckling, presented in Table I, and they are uniformly distorted (see Fig. 3). It is revealed that for the 1×1 unit cell, only one conformer (chair-like) of hydrogen is possible. It is clear that only C_{11} can be represented by both 1×1 unit cell and 2×1 supercell sizes. We also see in Fig. 4 that these configurations (C_7-C_9 and C_{11}) have nearly the same formation energies per atom. As presented in Fig. 5, all the functionals predict that these configurations also have nearly the same interlayer distance. When comparing the functionals, it is noted that GGA-PBE gives the highest interlayer spacing, whereas the vdW-DF2-C09$_x$ yields the lowest.

When comparing configurations C_{11}-C_{16}, it is seen in Fig. 4 that C_{11} is more energetically favorable whereas C_{12} has the highest formation energies. We therefore suggest that configuration C_{11} represents a possible template that can be used for hydrogen storage. The formation energies of configurations C_{14}-C_{16} are between those for C_{11} and C_{12}. This is due to the fact that they are made up of pair combinations of the conformers. The highest formation energy found for C_{12} is in contrast with the findings of Leenaerts *et al.*[62] for their studies of a similar kind of hydrogen arrangement on 2×1 single layer graphene. They found that a structure similar to configuration C_{12} is lower in formation energy compared to that of C_{13}. In this work, we have examined similar configurations on 2×1 single layer graphene, and our results show the same trend as theirs[62]. When 2×1 bilayer graphene is considered, the trend alters. Interestingly, when the interlayer distance of configurations C_{11}-C_{13} is fixed at 7 Å, analysis of the formation energies shows the same trend as the hydrogenated single layer graphenes (C_{13}>C_{12}>C_{11}). When the structures are allowed to relax to their equilibrium interlayer distance the trend changes to C_{12}>C_{13} >C_{11}, which tells us that there is a possible interaction between the hydrogen decorated planes that greatly affects the energetics of the structures.

The stability observed in C_{11}-C_{16} is ascribed to the hydrogen induced puckering mechanism on both layers which was also observed by Sofo *et al.*[50] The relaxed structures show that all the carbon atoms are hydrogenated and the graphene layers are buckled (moved up and down out of the planes). Mainly, this buckling occurs during the wavefunction overlap between the carbon and hydrogen atoms resulting in all the carbon atoms having sp^3 re-hybridization. It is noted in configurations C_{11}-C_{13} that the hydrogen atoms are differently aligned after relaxation, and it is also shown in Table I that C_{11} is uniformly distorted whereas C_{12} and C_{13} are non-uniformly distorted (see Fig. 3).

To quantify the distortions induced by hydrogen adatoms on the 2×1 supercell of bilayer graphene, the distances (l_a,l_s) and angles (θ_a, θ_s) between the carbon atoms are measured,and presented in Table III. Since l_s and θ_s are not measurable in C_{11}, this tells us that the structural properties deviate constantly for the entire structure unlike in C_{12} and C_{13}. We see in C_{12} that all the exchange correlation functionals predict that l_a stretches more than l_s, which is a confirmation that the hydrogen atoms are responsible for the non-uniform distortions in the structure. This observation is not always the case for all configurations because in C_{13} the distance l_s is more than l_a. This implies that the different arrangements of hydrogen atoms result in different deviations in structural pa-

rameters, where we suspect the possible hydrogen-hydrogen interactions that lead to bending of hydrogen atoms in C_{12} and C_{13} but not in C_{11} (see Fig. 3). It is important to note in Table III that each distance stretches towards a value that is close to that of cubic diamond value (1.53 Å) and their corresponding angle deviates towards the ideal tetrahedral internal angle.

Even if it is known that in configurations C_{11}-C_{16}, all the carbon atoms are saturated resulting in the minimal π-π interactions between the hydrogen layers, it is seen on Fig. 5 that all the functionals vary in predicting the equilibrium interlayer distances (d_0). GGA-PBE gives the largest d_0 whereas vdW-DF-C09$_x$ gives the lowest. It is also observed on Fig. 5 that the d_0 greatly depends on the arrangement of hydrogen adatoms. We see that configuration C_{12}, which is greatly distorted by the hydrogen atoms, has the shortest d_0 compared to the other configurations.

C. Elastic properties

We now look at the elastic properties of the most energetically favorable configuration C_9. The values for the elastic constants and derived elastic moduli for all four functionals considered are given in Table. IV as well as those for graphene, bilayer graphene and graphane. Since these structures are all isotropic, they only have two independent elastic constants, namely c_{11} and c_{12} which can be calculated by separately applying an isotropic bi-axial strain and an area conserving strain.

From these the following elastic properties are defined

$$\begin{aligned} Y &= c_{11} - \frac{c_{12}^2}{c_{11}} \\ G &= c_{66} = \frac{c_{11} - c_{12}}{2} \\ \nu &= \frac{c_{12}}{c_{11}} \end{aligned} \tag{2}$$

where Y is the 2D Young's modulus (in-plane stiffness), G is the 2D shear modulus and ν is the Poisson ratio.

The results in Table. IV show that in the case of graphane and C_{11}, the elastic constants and modulus values increase from vdW-DF→GGA-PBE→vdW-DF2-C09$_x$ →vdW-DF-C09$_x$. The Poisson ratios remain more or less constant for all four functionals. The results of Cadelano *e*t al.[64] are comparable to our values for graphene and graphane with a slight discrepancy in c_{12} for graphane which results in a lower value of 0.08 for the Poisson ratio. The bilayered structures have values for the elastic constants and moduli which are approximately twice that of their monolayer counterparts. This is expected since the two layers are very weakly bound. The effect of hydrogenation is too reduce the elastic values of the pristine structures. For the elastic constants, c_{11} approximately reduces by a factor of 0.7 whereas c_{12} reduces by 0.40~0.43. This results in the moduli reducing by approximately 0.70~0.78. The effect of the added adatoms is to significantly reduce the strength of the pristine structures.

IV. CONCLUSIONS

In this study, we investigated all hydrogen configurations that can possibly exist on a 1×1 unit cell of bilayer graphene at 100% coverage where each carbon contains an hydrogen adatom in the unrelaxed state. Thereafter the cell was increased to a 2×1 supercell to show other configurations that are not possible for a 1×1 unit cell. All the exchange correlation functionals predict that, of the ten identified configurations obtained from the 1×1 unit cell, nine are energetically favorable. The three lowest energy competing geometries (configurations C_7-C_9) are identified. We notice that in the case of physisorbed H_2 dimer, the coupled structures are more energetically stable than the decoupled configurations.

In the case of a 2×1 supercell, only the six energetically favorable configurations are presented in this work. In these configurations, it is found that all hydrogen atoms are attached to the substrate after relaxation. In some of the configurations, it is found that the arrangement of hydrogen atoms greatly distort the hexagonal layer to such an extent, the $C-C$ bond distances are unequal. We notice that one of the identified configurations (C_{11}) exists both in 1×1 and 2×1 cells, and is the most energetically stable structure. We therefore suggest that this configuration represents a possible template that can be used for hydrogen storage.

Our results tells us that there is a possibility of interaction between the hydrogen decorated planes that greatly affects the energetics of the structures. The effect of the hydrogen adatoms greatly reduces the strength of the bilayer graphene structures.

In conclusion, it is seen that the functionals vary in predicting the various properties. The vdW-DF-C09$_x$ functional predicts the lowest formation energies and shortest interlayer distances for all configurations considered, whereas the GGA-PBE functional predicts highest formation energies and largest interlayer distances. In the case of the moduli results, vdW-DF gives the smallest values, whereas the vdW-DF-C09$_x$ gives the largest values.

ACKNOWLEDGMENTS

The authors would like to thank the University of Pretoria for computational resources and financial support. REM acknowledges the financial support from the National Research Foundation (NRF). NC and RCA are grateful to the National Institute of Theoretical Physics for financial support.

* edwin.mapasha@up.ac.za

† richard.andrew@up.ac.za

[1] M. Dion, H. Rydberg, E. Schroder, D. C. Langreth, and B. I. Lundqvist, Phys. Rev. Lett. **92**, 246401 (2004).
[2] O. A. von Lilienfeld, I. Tavernelli, U. Rothlisberger,D. Sebastiani, Phys. Rev. Lett. **93**, 153004 (2004).
[3] J. Antony, and S. Grimme, Phys. Chem. Chem. Phys. **8**, 5287 (2006).
[4] A. D. Becke, and E. R. Johnson, J. Chem. Phys. **127**, 154108 (2007).
[5] S. Grimme, J. Antony, T. Schwabe, and C. Muck-Lichtenfeld, Org. Biomol. Chem. **5**, 741 (2007).
[6] T. Sato, T. Tsuneda, and K. Hirao, J. Chem. Phys. **126**, 234114 (2007).
[7] A. Tkatchenko and M. Scheffler, Phys. Rev.Lett. **102**, 073005 (2009).
[8] Y. Zhang and W. Yang, Phys. Rev. Lett. **80**, 890 (1998).
[9] G. Roman-Perez and J. M. Soler, Phys. Rev. Lett. **103**, 096102 (2009).
[10] J. Klimes, D. R. Bowler, and A. Michaelides, J. Phys. Condens. Matter **22**, 022201 (2010).
[11] V. R. Cooper, Phys. Rev. B **81**, 161104 (2010).
[12] I. Hamada and M. Otani, Phys. Rev. B **82**, 153412 (2010).
[13] K. Lee, E. D. Murray, L. Kong, B. I. Lundqvist, and D. C. Langreth, Phys. Rev. B **82**, 081101 (2010).
[14] E. D. Murray, K. Lee, and D. C. Langreth, J. Chem. Theory Comput. **5**, 2754 (2009).
[15] K. S. Novoselov, A. K. Geim, S. V. Morozov, D. Jiang, Y. Zhang, S. V. Dubonos, I. V. Grigorieva, and A. A. Firsov, Science **306**, 666 (2004).
[16] A. K. Geim and K. S. Novoselov, Nature Mater. **6**, 183 (2007).
[17] P. R. Wallace, Phys. Rev. **71**, 622 (1947).
[18] K. S. Novoselov, A. K. Geim, S. V. Morozov, D. Jiang, Y. Zhang, M. I. Katsnelson, S. V. Dubonos, I. V. Grigorieva, and A. A. Firsov, Nature (London) **438**, 197 (2005).
[19] K. S. Novoselov, Z. Jiang, Y. Zhang, S. V. Morozov, H. L. Stormer, U. Zeitler, J. C. Maan, G. S. Boebinger, P. Kim, and A. K. Geim, Science **315**, 1379 (2007).
[20] Y. Zhang, Y. W. Tan, H. L. Stormer, and P. Kim, Nature (London) **438**, 201 (2005).
[21] A. H. Castro, F. Guinea, N. M. R. Peres, K. S. Novoselov, and A. K. Geim, Rev. Mod. Phys. **81**, 109 (2009).
[22] F. Schedin, A. K. Geim, S. V. Morozov, E. W. Hill, P. Blake, M. I. Katsnelson, and K. S. Novoselov, Nature Mater. **6**, 652 (2007).
[23] W. Choi, I. Lahiri, R. Seelaboyina, and Y. S. Kang, Crit. Rev. Solid State and Mater Sci. **35**, 52 (2010).
[24] H. Min and A. H. MacDonald, Phys. Rev. B **77**, 155416 (2008).
[25] T. Ohta, A. Bostwick, T. Seyller, K. Horn, and E. Rotenberg, Science **313**, 951 (2006).
[26] L. Sun, Q. X. Li, H. Ren, H. B. Su, Q. W. Shi, and J. L. Yang, J. Chem. Phys **129**, 074074 (2008).
[27] Y. W. Son, M. L. Cohen, and S. G. Louie, Phys. Rev. Lett **97**, 216803 (2006).
[28] M. Y. Han, B. Ozyilmaz, Y. Zhang, and P. Kim, Phys. Rev. Lett **98**, 206805 (2007).
[29] F. Ding, Phys. Rev. B **72**, 245409 (2005).
[30] G. D. Lee, C. Z. Wang, E. Yoon, N. M. Hwang, D. Y. Kim, and K. M. Ho, Phys. Rev. Lett. **95**, 205501 (2005).
[31] M. T. Lusk and L. D. Carr, Phys. Rev. Lett. **100**, 175503 (2008).
[32] S. C Pradhan and J. K. Phadikar, Phys. Lett. A **373**, 1062 (2009).
[33] P. Lu, Z. Zhang, and W. Guo, Phys. Lett. **373**, 3354 (2009).
[34] Z. Q. Luo, T. Yu, K. J. Kim, Z. H. Ni, Y. M. You, S. H. Lim, Z. X. Shen, S. Z. Wang, and J. Y. Lin, ACSNANO **3**, 1781 (2009).
[35] Y. H. Lu, W. Chen, Y. P. Feng, and P. M. He, J. Phys. Chem. B **113**, 2 (2009).
[36] I. Zanella, S. Guerini, S. B. Fagan, J. MendesFilho, and A. G. SouzaFilho, Phys. Rev. B **77**, 073404 (2008).
[37] R. M. Ribeiro, N. M. R. Peres, J. Coutinho, and P. R. Briddon, Phys. Rev. B **78**, 075442 (2008).
[38] D. W. Boukhvalov, M. I. Katsnelson, and A. I. Lichtenstein, Phys. Rev. B **77**, 035427 (2008).
[39] S. Lebegue, M. Klintenberg, O. Eriksson, and M. I. Katsnelson, Phys. Rev. B **79**, 245117 (2009).
[40] E. J. Duplock, M. Scheffler, and P. J. D. Lindan, Phys. Rev. Lett. **92**, 225502 (2004).
[41] D. W. Boukhvalov and M. I. Katsnelson, Phys. Rev. B **78**, 085413 (2008).
[42] N. Z. Lu, Z. Y. Li, and J. L. Yang, J. Phys. Chem. C **113**, 16741 (2009).
[43] J. A. Yan, L. Xian, and M. Y. Chou, Phys. Rev. Lett. **103**, 086802 (2009).
[44] X. S. Wu, M. Sprinkle, X. B. Li, F. Ming, C. Berger, and W. A. de Heer, Phys. Rev. Lett. **101**, 026801 (2008).
[45] I. Jung, D. A. Dikin, R. D. Piner, and R. S. Ruoff, Nano Lett. **8**, 4283 (2008).
[46] Z. Luo, P. M. Vora, E. J. Mele, A. T . C. Johnson, and J. M. Kikkawa, Appl. Phys. Lett. **94**, 111909 (2009).
[47] R. Balog, B. Jorgensen, L. Nilsson, M. Andersen, E. Rienks, M. Bianchi, M. Fanetti, E. Laegsgaard, A. Baraldi, S. Lizzit, Z. Sljivancanin, F. Besenbacher, B. Hammer, T. G. Pedersen, P. Hofmann, and L. Hornekaer. Nature Mater. **9**, 315 (2010).
[48] A. Savchenko, Science **323**, 589 (2009).
[49] D. C. Elias, R. R. Nair, T. M. G. Mohiuddin, S. V. Morozov, P. Blake, M. P. Halsall. A. C. Ferrari, D. W Boukhvalov, M. I. Katsnelson, A. K. Geim, and K. S. Novoselov, Science. **323**, 610 (2009).
[50] J. O. Sofo, A. S. Chaudhari, and G. D. Barber, Phys. Rev. B **75**, 153401 (2007).
[51] K. S. Subrahmanyam, P. Kumar, U. Maitra, A. Govindaraj, K. P. Hembram, U. V. Waghmare, and C. N. R. Rao, Proc. Nat. Acad. Sci. (USA) **108**, 2677 (2011).
[52] M. Jaiswal, C. H. Lim, Q. Bao, C. T. Toh, K. P. LOh, and B. Ozyilmaz, ACSNANO **5**, 888 (2011).
[53] L. Wang, N. R. Stuckert, and R. T. Yang, AIChE, **57**, 10 (2011).
[54] O. Leenaerts, B. Partoens, and F.M. Peeters, Phys. Rev. B **80**, 245422 (2009).
[55] R. E. Mapasha, A.M. Ukpong, and N. Chetty, Phys. Rev. B **85**, 205402 (2012).
[56] J. Rohrer, and P. Hyldgaard, Phys. Rev. B **83**, 165423 (2011).
[57] P. E. Blochl, Phys. Rev. B **50**, 17953 (1994).
[58] P. Giannozzi, S. Baroni, N. Bonini, M. Calandra, R. Car, C. Cavazzoni, D. Ceresoli, G. L. Chiarotti, M. Cococcioni, I. Dabo, A. Dal Corso, S. Fabris, G. Gougoussis, A. Kokalj, M. Lazzeri, L. Martin-Samos, N. Marzari, F. Mauri, R. Mazzarello, S. Paolini, A. Pasquarello, L. Paulatto, C. Sbraccia, S. Scandolo, G. Sclauzero, A. P. Seitsonen, A. Smogunov, P. Umari, and R. M. Wentzcovitch, J. Phys. Condens. Matter **21**, 395502 (2009).
[59] J. P. Perdew, K. Burke, and M. Ernzerhof, Phys. Rev. Lett. **77**, 3865 (1996).
[60] H. J. Monkhorst and J. D. Pack, Phys. Rev. B **13**, 5188 (1976).
[61] See Table SIV in the supplementary material of[12]. Available online at: http://link.aps.org/supplemental/10.1103/PhysRevB.82.153412
[62] O.Leenaerts, H. Peelaers, A. D. Hernandez-Nieves, B. Partoens, F. M. Peeters, Phys. Rev. B **82**, 195436 (2010)
[63] D. Henwood and J. D. Carey, Phys. Rev **75**, 245413 (2007).
[64] E. Cadelano, P. L. Palla, S. Giordano and L. Colombo, Phys. Rev. B. **82**, 235414 (2010).

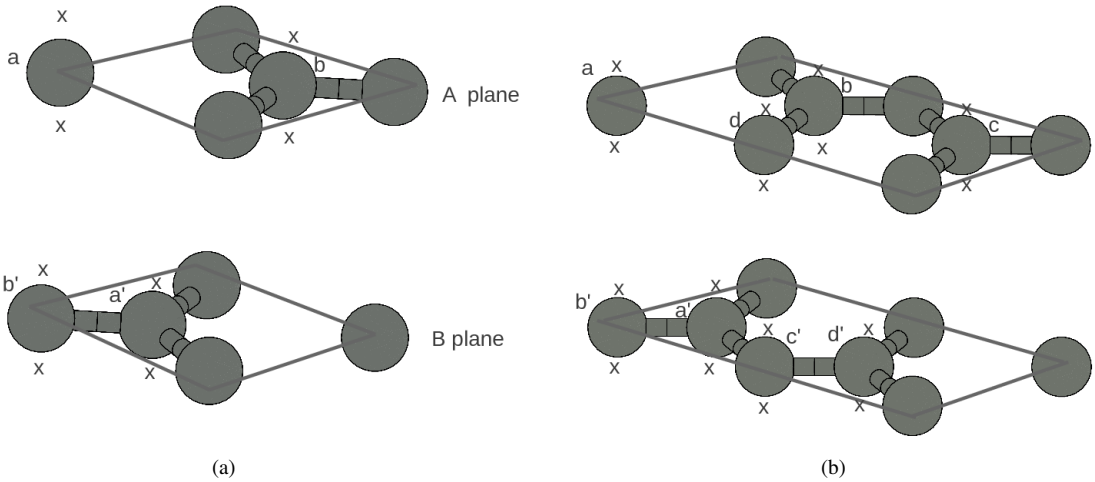

FIG. 1: The adsorption sites for hydrogen atoms on (a) 1×1 and (b) 2×1 cells of bilayer graphene. The labels on top and bottom layers depict the distinct carbon atoms on the AB stacked bilayer graphene. The letter x shows the exact positions of hydrogen atoms before relaxation.

TABLE I: The hydrogen configurations on 1×1 and 2×1 supercell bilayer graphene at 100% coverage in the unrelaxed states. The subscripts *a* and *b* refer to positions above and below the adsorption sites, respectively, and B_u and B_n represent uniform and non-uniform buckled configurations.

Cell size	Index	Hydrogen configurations		Structural distortion		Formation of H_2
		PlaneA	PlaneB	PlaneA	PlaneB	
1×1	C_1	$a_a b_a$	$a'_a b'_a$	Flat	Flat	Formed
	C_2	$a_a b_a$	$a'_b b'_b$	Flat	Flat	Formed
	C_3	$a_b b_a$	$a'_a b'_a$	B_u	Flat	Formed
	C_4	$a_a b_b$	$a'_a b'_a$	B_u	Flat	Formed
	C_5	$a_b b_a$	$a'_b b'_b$	B_u	Flat	Formed
	C_6	$a_a b_b$	$a'_b b'_b$	B_u	Flat	Formed
	C_7	$a_b b_a$	$a'_b b'_a$	B_u	B_u	None
	C_8	$a_b b_a$	$a'_a b'_b$	B_u	B_u	None
	C_9	$a_a b_b$	$a'_a b'_b$	B_u	B_u	None
	C_{10}	$a_b b_b$	$a'_a b'_a$	B_n	B_n	Formed
2×1	C_{11}	$a_b b_a c_a d_b$	$b'_b a'_a c'_b d'_a$	B_u	B_u	None
	C_{12}	$a_a b_b c_a d_b$	$b'_a a'_a c'_b d'_b$	B_n	B_n	None
	C_{13}	$a_b b_b c_a d_a$	$b'_b a'_a c'_a d'_b$	B_n	B_n	None
	C_{14}	$a_a b_b c_a d_b$	$b'_b a'_a c'_b d'_a$	B_n	B_u	None
	C_{15}	$a_a b_b c_a d_b$	$b'_b a'_a c'_a d'_b$	B_n	B_n	None
	C_{16}	$a_b b_a c_a d_b$	$b'_b a'_a c'_a d'_b$	B_u	B_n	None

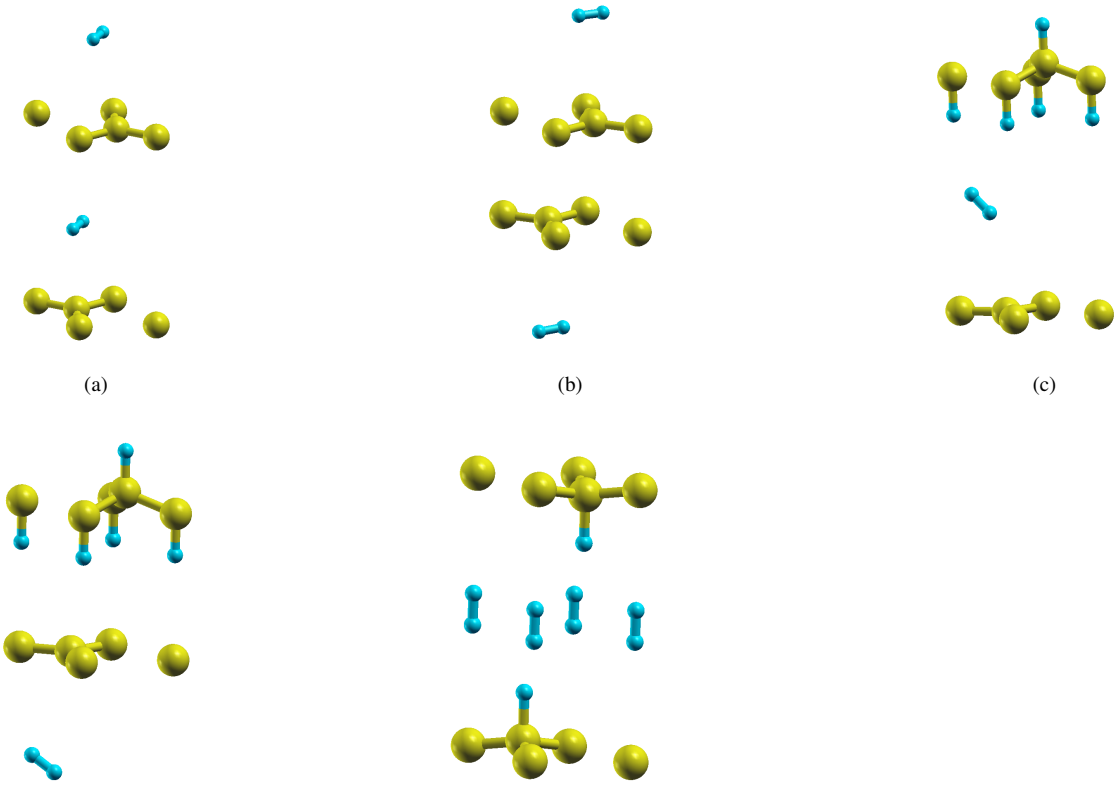

FIG. 2: The selected relaxed configurations showing the H_2 dimers physisorbed and atomic hydrogen chemisorbed on 1×1 unitcell bilayer graphene: (a) C_1, (b) C_2, (c) C_3,(d) C_5, (e) C_{10}.

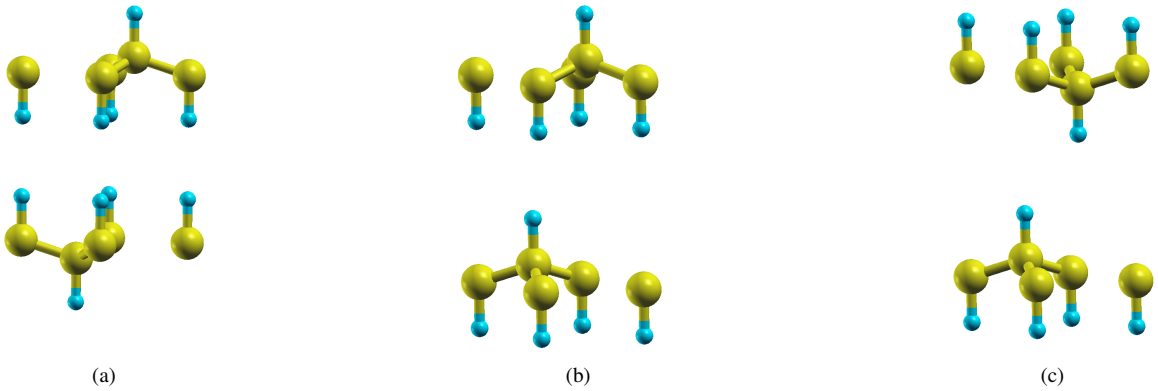

(a) (b) (c)

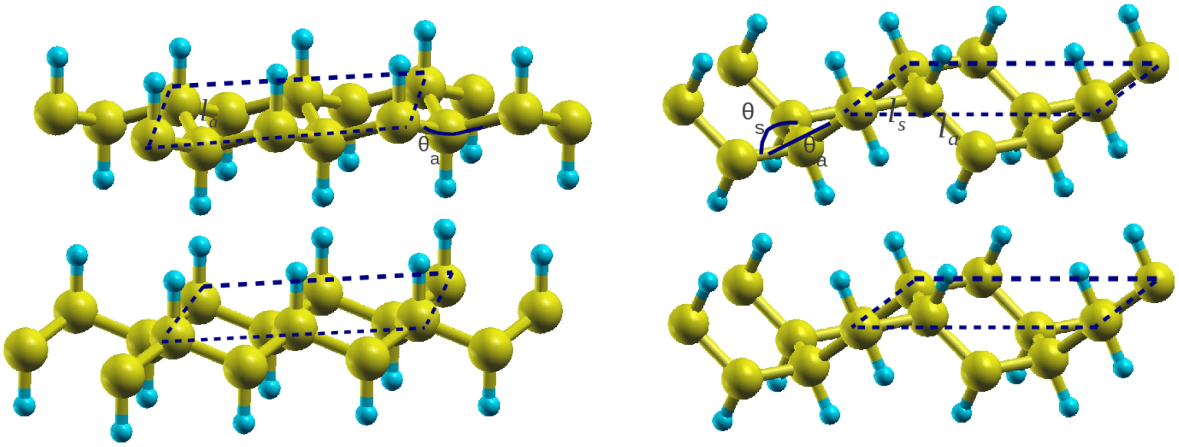

(d) (e)

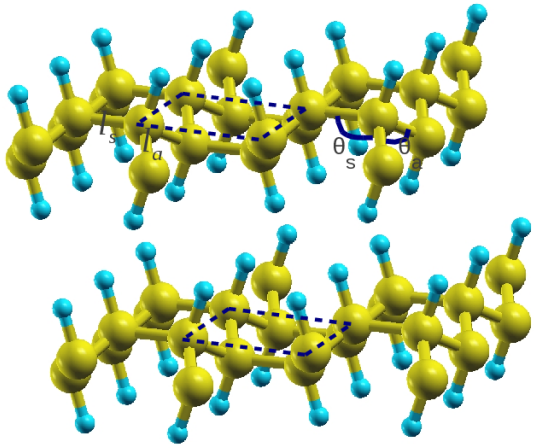

(f)

FIG. 3: The relaxed geometries of the three lowest energy competing configurations identified from a 1×1 unit cell: (a) C_7, (b) C_8, (c) C_9. Configurations (d) C_{11}, (e) C_{12}, and (f) C_{13} are selected geometries that are only possible for a 2×1 supercell. The dashed parallelograms show the 2×1 supercell that contains four carbon atoms per plane. The distances l_s and l_a are the distinct distances between the carbon atoms with the hydrogen atoms adsorbed on the same side or in an alternating pattens, respectively. Similar for the angles.

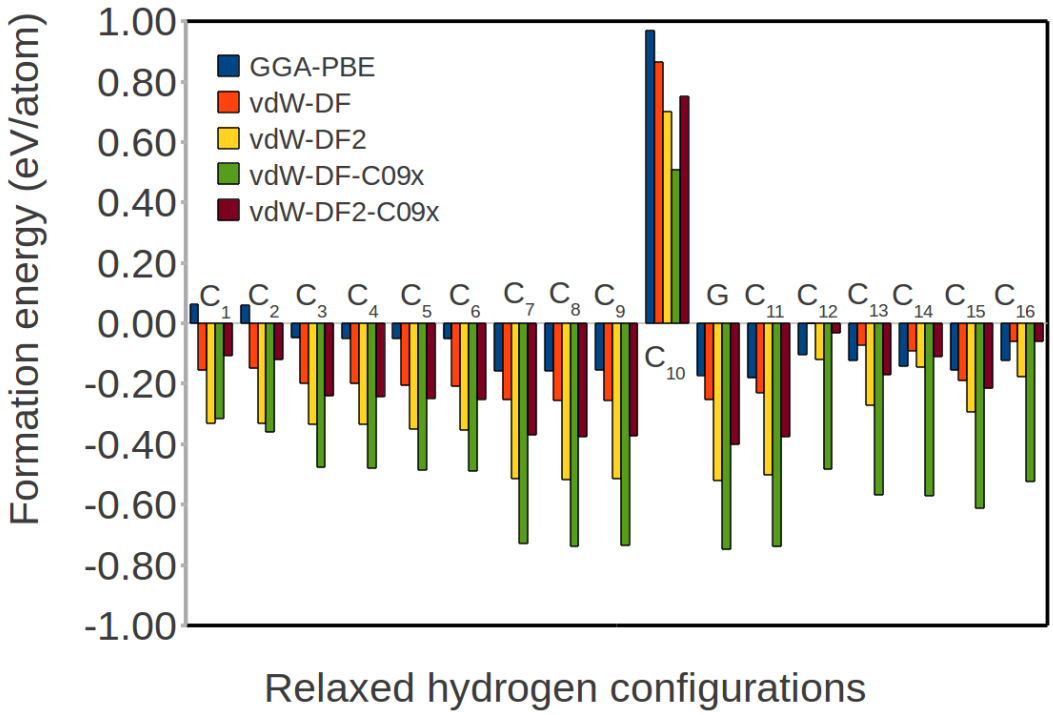

FIG. 4: The variation of formation energies with respect to identified configurations from 1×1 and 2×1 cells predicted by GGA-PBE, vdW-DF, vdW-DF2, vdW-DF-C09$_x$ and vdW-DF2-C09$_x$ functionals. The letter G stands for 1×1 graphane.

TABLE II: The calculated equilibrium distances d_{C-H_2} (in Å) between the hexagonal layers of 1×1 bilayer graphene and H_2 dimer for the selected configurations. The distance d_{C-H_2} is considered to be measured when the H_2 dimer is either inside (I) or outside (O) the bilayer graphene.

Functionals	Position	C_1	C_2	C_3	C_5	C_{10}
GGA-PBE	I	3.93		3.91		3.86
	O	3.98	3.96		3.99	
vdW-DF	I	3.00		3.01		3.50
	O	3.05	3.08		3.09	
vdW-DF2	I	2.86		2.90		3.31
	O	2.98	3.02		2.97	
vdW-DF-C09$_x$	I	2.78		2.82		2.98
	O	2.86	2.85		2.86	
vdW-DF2-C09$_x$	I	2.81		2.81		2.73
	O	2.87	2.87		2.85	

TABLE III: The calculated structural properties of the selected configurations obtained from 2×1 supercell bilayer graphene using the five exchange correlation functionals. The distances l_s and l_a are the distinct distances between the carbon atoms where the hydrogen atoms are adsorbed on the same side or in an alternating pattens, respectively. Similar for the angles.

Functionals	C_{11}		C_{12}		C_{13}		C_{11}		C_{12}		C_{13}	
	l_a	l_s	l_a	l_s	l_a	l_s	θ_a	θ_s	θ_a	θ_s	θ_a	θ_s
GGA-PBE	1.53		1.59	1.54	1.52	1.57	110.8		117.3	106.9	109.4	112.5
vdW-DF	1.51		1.59	1.54	1.53	1.57	109.9		116.7	106.0	108.4	116.8
vdW-DF2	1.51		1.60	1.55	1.52	1.56	110.1		117.2	106.4	108.6	112.5
vdW-DF-C09$_x$	1.51		1.58	1.55	152	1.56	110.1		117.5	106.2	108.8	112.65
vdW-DF2-C09$_x$	1.51		1.58	1.54	1.52	1.55	110.1		117.5	106.6	108.6	112.9

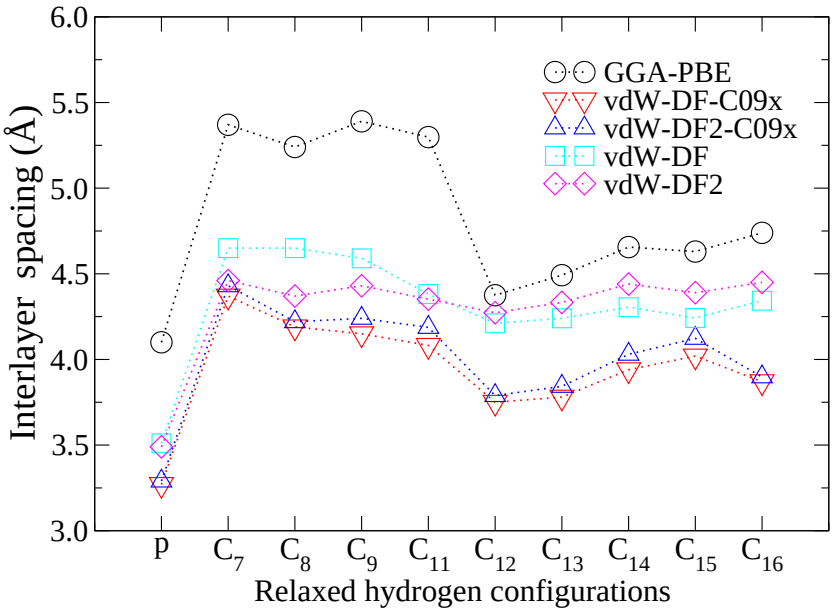

FIG. 5: The calculated equilibrium interlayer distances d_0 (in Å) for the lowest energy competing configurations identified from 1×1 and 2×1 cells. The letter P stands for pristine bilayer graphene.

TABLE IV: Elastic properties for pristine and hydrogenated single and bi-layered graphene (Elastic constants c_{ij}, shear modulus G and in-plane stiffness Y in Nm^{-1}. Poisson ratio ν (dimensionless)).

		c_{11}	c_{12}	G	Y	ν
Graphene	GGA-PBE	354.4	62.1	146.2	343.5	0.175
	vdW-DF	346.0	58.2	143.9	336.2	0.168
	vdW-DF-C09$_X$	355.7	64.9	145.4	343.8	0.182
	vdW-DF2-C09$_X$	354.5	63.9	145.3	343.0	0.180
	GGA-PBE-PW91[a]	354	60	147[b]	344[b]	0.17[b]
bilayer graphene	GGA-PBE	708.3	126.0	291.2	685.9	0.178
	vdW-DF	690.5	117.1	286.7	670.6	0.170
	vdW-DF-C09$_X$	707.1	134.2	286.5	681.6	0.190
	vdW-DF2-C09$_X$	702.5	134.8	283.9	676.6	0.180
Graphane (100%)	GGA-PBE	245.4	25.0	110.2	242.9	0.102
	vdW-DF	236.4	23.0	106.7	234.2	0.097
	vdW-DF-C09$_X$	251.4	27.8	111.8	248.3	0.111
	vdW-DF2-C09$_X$	248.3	28.1	110.1	245.1	0.113
	GGA-PBE-PW91[a]	248	20	114[b]	246[b]	0.08[b]
C_9	GGA-PBE	489.9	51.2	219.4	484.5	0.105
	vdW-DF	473.3	44.5	214.4	469.1	0.094
	vdW-DF-C09$_X$	502.5	55.6	223.5	496.3	0.111
	vdW-DF2-C09$_X$	497.0	55.1	221.0	490.9	0.111

[a] Reference[64]
[b] Elastic properties derived from their elastic constants